Experimental report of proposal HC-3386, by Knibbe J.S.

Beamtime session at beamline id27 from 24-01-2018 until 30-01-2018

Team: Knibbe, J. S., Luginbuhl, S., Van Hoolst, T., Charlier, B., Namur, O., van Westrenen, W., Sifre, D., and Mezouar, M.

1 Introduction

Density measurements of Fe-Si-C liquid metals are performed on a Paris-Edinburgh (PE) press using X-ray absorption techniques at beamline ID-27 of the European Synchrotron Radiation Facility in Grenoble, France. Pressure is applied to the PE assembly (van Kan Parker et al., 2010) by increasing the oil pressure of the hydraulic press to either 300 bar, 400 bar, or 500 bar. Subsequently, the temperature is increased in steps to superliquidus conditions by ohmic dissipation in a graphite furnace using a DC power supply. In-between heating steps, X-ray spectra are collected of the sample to check whether the sample is liquid or solid. X-ray spectra of the BN and Pt calibrant material are collected to estimate pressure and temperature from isochore crossings of the obtained unit cell volumes according to equations of state (EOSs) of BN and Pt (section A4). When the X-ray spectra of the sample confirm that the sample is molten, one or multiple horizontal X-ray absorption profiles of the assembly are collected. An absorption profile is collected by moving the assembly in horizontal direction through the X-ray beam, while photodiodes measure the beam intensity in front of (I_0) and behind (I) the assembly. These X-ray absorption profiles are used to estimate the X-ray absorption by the sample at experimental conditions $\left(\rho_{S,PT}\mu_S\right)$ (section 2.3). After the experiment is quenched and decompressed, additional horizontal X-ray absorption profiles of the assembly (A) including the diamond (D) container and sample (S) (D+S+A) are acquired at ambient pressure and temperature conditions. X-ray absorption profiles of exclusively the diamond containing the sample (D+S) after recovering them from the assembly are also acquired. These D+S+A and D+S X-ray absorption profiles are used to estimate the absorption by the sample at ambient conditions $\left(\rho_{S,0}\mu_S\right)$ (section 2.2). The samples are recovered from the diamond, and their densities at ambient conditions $\left(\rho_{S,0}\right)$ are measured by hydrostatic weighing at the IPGP in Paris, France (section 3). Samples that are recovered from experiments that are performed with identical starting composition are assumed to have identical density at ambient conditions, such that these samples could be weighed simultaneously. This is needed to increase the accuracy of the hydrostatic weighing and to estimate the density of tiny samples that were unsuccessfully recovered from the diamond container (section 3). The results are integrated in a research article about Mercury's interior structure (Knibbe et al., 2020).

2 Analysis of X-ray absorption profiles

2.1 Description of X-ray absorption profiles

The absorption of X-rays between the photodiodes as a function of the assembly's position *x* on a horizontal line *X* that is orthogonal to the X-ray beam is given by the Beer-Lambert law

$$ln\left(\frac{I(x)}{I_0(x)}\right) = C - \rho_A\mu_A\delta_A(x) - \rho_D\mu_D\delta_D(x) - \rho_S\mu_S\delta_S(x), \qquad (A2)$$

with ρ_i density, μ_i the mass absorption coefficient, and, by cylindrical geometry of the assembly, diamond, and sample,

$$\delta_i(x) = 2\sqrt{{r_{i,out}}^2 - (x - x_0)^2} - 2\sqrt{{r_{i,in}}^2 - (x - x_0)^2}, \quad (A3)$$

describing the pathlength through the assembly ($i = A$), diamond ($i = D$) or sample ($i = S$). In equation A3, $r_{i,in}$ and $r_{i,out}$ denote the inner and outer radius, respectively, of part i. Parameter C captures the relative difference in gain between the two photodiodes as well as the absorption due to air. Parameter C consistently takes values of ~ -1.17 for the data collected in this study. The X-coordinate of the beam's centre is denoted by x_0.

Each absorption profile consists of 200 measurements $\left\{X(x_1) = ln\left(\frac{I(x_1)}{I_0(x_1)}\right), X(x_2) = ln\left(\frac{I(x_2)}{I_0(x_2)}\right), \ldots, X(x_{200}) = ln\left(\frac{I(x_{200})}{I_0(x_{200})}\right)\right\}$, collected with an 0.1 mm^2 X-ray beam (33.2 keV). The dimensions of the X-ray beam are controlled by vertical and horizontal slits. The 200 measurements are collected while moving the assembly in X-direction with a step size of 0.01 mm (i.e. $x_j - x_{j-1} = 0.01$mm). The data are modelled by

$$X(x) = f(\beta, x) + R(x), \qquad (A4)$$

with

$$f(\beta, x) = \frac{\int_{-L/2}^{L/2}(C - \rho_A\mu_A\delta_A(x) - \rho_D\mu_D\delta_D(x) - \rho_S\mu_S\delta_S(x))dx}{L} + R(x)\,. \quad (A5)$$

In this equation, L is the beam width, R are the residuals, and

$$\beta = \left\{L, C, \rho_A\mu_A, \rho_D\mu_D, \rho_S\mu_S, r_{A,out}, r_{A,in} = r_{D,out}, r_{S,out} = r_{D,in}, x_0\right\}$$

is the set of parameters that describe the collected absorption profile (equations A3 and A5). The D+S profiles are collected of the sample in the diamond container after recovering from the assembly, which reduces the number of parameters ($\rho_A\mu_A = 0$ and $r_{A,out} = 0$). The parameters are fitted to the measurements by a nonlinear least squares regression procedure (text F). Below, we describe the specific procedure of fitting these parameters to the absorption profiles collected at ambient conditions (section 2.2) and *in situ* (section 2.3) in detail.

2.2. Fitting of parameters to X-ray absorption profiles that are collected at ambient conditions

Because it is assumed that samples recovered from experiments of the same starting composition have the same density at ambient conditions (section 3 of this text) and because μ_S only depends on composition, it follows that $\rho_{S,0}\mu_S$ are identical among samples with the same starting composition. As a consequence, $\rho_{S,0}\mu_S$ needs to be determined by fitting Beer-Lambert formulations to all profiles at ambient pressure that are collected on samples that share their starting composition in a single fit. To reduce the number of free parameters, parameters L, C, and $r_{A,out}$ are also assumed identical among ambient absorption profiles collected from samples with the same starting composition. In practice, the diameter of the post-experimental assembly ($r_{A,out}$) can vary between experiments as a result of the different amounts of vertical compression that experimental assemblies have been exposed to. However, by fitting individual values of $\rho_A\mu_A$ to each absorption profile, variations in the characteristics of assembly material per experiment are sufficiently considered. Parameters $\rho_D\mu_D$ and $r_{D,out}$ are allowed to have different value per experiment, but these are assumed equal among the D+S+A and D+S absorption profiles of an identical experiment, because we do not expect the diamond to deform at ambient conditions by removing it from the assembly. Separate values of $r_{S,out} = r_{D,in}$ and of x_0 are fitted to each absorption profile.

Figure 1 presents the fit to the D+S+A and D+S ambient pressure absorption data of exp5, exp6 and exp7, which are performed with identical starting material (Fe-17wt%Si). As described above, parameters $\rho_S\mu_S, L,\ C,$ and $r_{A,out}$ are considered constant among the profiles (four parameters), separate values for $\rho_A\mu_A$ are fitted to each of the three D+S+A profiles (three parameters), separate values of $\rho_D\mu_D$ and $r_{D,out}$ are fitted to profiles of each experiments but are considered to be equal among D+S+A and D+S absorption profiles of the identical experiment (six parameters), and for each of the six absorption profiles, individual parameters of $r_{S,out} = r_{D,in}$ and x_0 are adopted (twelve parameters). In total, 25 parameters are simultaneously fitted to the six absorption profiles.

An enhanced absorption due to the MgO-Pt calibrant mixture that is placed at the outside of the diamond is detected in the D+S+A absorption profiles (figure 1). Additional outliers are present in the D+S absorption profile of Exp5, which are potentially due to traces of MgO-Pt powder that may have remained at the outside of the diamond after removing the diamond and sample from the assembly. These datapoints are excluded from the fitting because the absorption of calibrant powder is not modelled.

Table 2 lists the estimates of $\rho_{S,0}\mu_S$ at post-situ ambient conditions and the formal fitting errors. Figure 2 shows all ambient-pressure absorption profiles together with the fitted profiles.

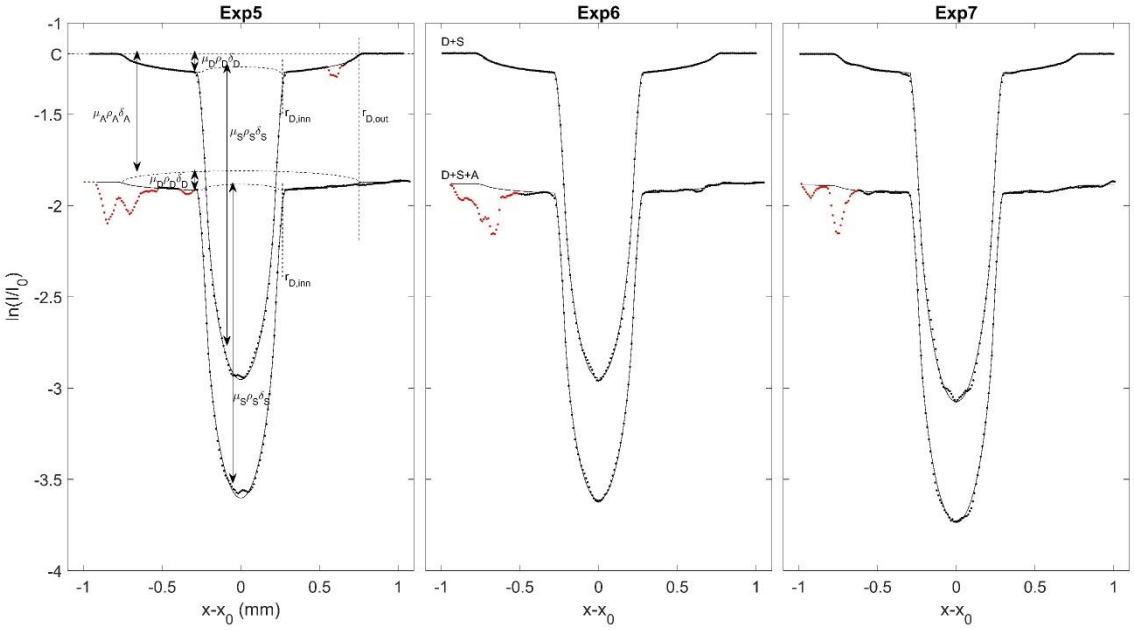

Figure 1. The ambient pressure X-ray absorption profiles of the assembly, diamond and sample (D+S+A) and of exclusively the diamond and sample (D+S) of the Exp5 (left), Exp6 (middle) and Exp7 (right) experiments (dots). The Beer-Lambert parametrization that is fitted to the data (solid line). Measurements that are affected by absorption of MgO+Pt calibrant powder are plotted in red and are excluded from the fit. Dashed lines in the left plot represent the separate components of the absorption (i.e. intensity differences by diode gain difference (C), assembly's absorption (A), diamond's absorption (D) and sample's absorption (S)). Raw data and the beer-lambert parametrisation are available online (Knibbe, 2020).

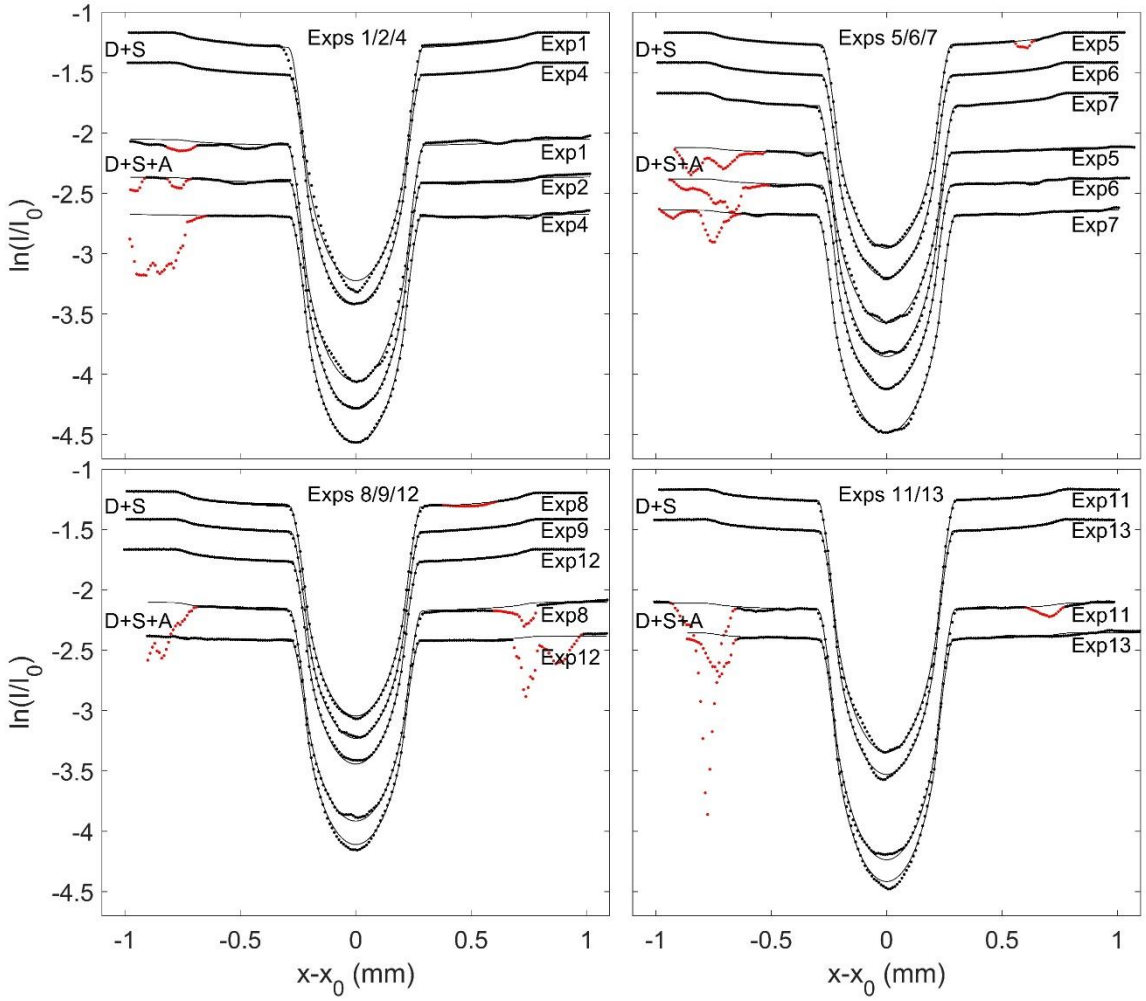

Figure 2. The ambient pressure X-ray absorption profiles (dotted) of the assembly, diamond and sample (D+S+A) and of exclusively the diamond and sample (D+S) of the four experimental sets that are performed with identical starting materials (Exp1-Exp2-Exp4, Exp5-Exp6-Exp7, Exp8-Exp9-Exp12, and Exp11-Exp13). The Beer-Lambert parametrisations that are fitted to the absorption profiles (lines). Measurements that are considered as outliers, of which most are affected by absorption of MgO+Pt calibrant powder, are plotted in red and are excluded from the fit. The profiles and the fits are artificially shifted in the figure by an additive constant in the Y-axis for illustrative purposes. Raw data and the beer-lambert parametrisation are available online (Knibbe, 2020).

2.3. Fitting of parameters to X-ray absorption profiles that are collected *in situ*

In many of the experiments performed in this study, we collected several absorption profiles directly after each other at separate altitudes through the sample at high pressure and superliquidus temperature (PT) conditions. We assume that $\rho_S\mu_S$ is identical among such PT absorption profiles of a single experiment because these absorption profiles are collected at identical pressure and temperature conditions. Accordingly, we estimate model parameters of the separate PT absorption profiles of an individual experiment in a single fit. Values of L, C, $r_{A,out}$, $r_{A,inn} = r_{D,out}$, and $\rho_D\mu_D$ are taken from Beer-Lambert fits to the ambient pressure absorption profiles of corresponding experiment, because these parameters are difficult to constrain from the PT absorption profiles. This is a reasonable assumption because the diamond capsule is far less compressible than the MgO, BN and boron epoxy parts that make up the assembly. We do consider individual values of $\rho_A\mu_A$, x_0 and $r_{D,inn} = r_{S,out}$ for each of the PT

absorption profiles. For several experiments, absorption profiles taken at a different altitude through the sample show significant differences in the inner radius of the diamond container ($r_{D,inn} = r_{S,out}$) which are likely related to deformation (e.g. bulging) of the inner part of the diamond cylinder under the applied vertical pressure. Figure 3 presents two such *in situ* absorption profiles of exp7, which are taken at a slightly different altitude trough the assembly. The difference in the amplitude and width of absorption features that are induced by the sample is completely ascribed to different inner radii of the diamond (0.2564 mm versus 0.2462mm) at the separate altitudes at which the profiles are collected.

The estimates of $\rho_S \mu_S$ at PT conditions are listed in table 1. Figure 4 shows the collected data and Beer-Lambert fits of all PT absorption profiles.

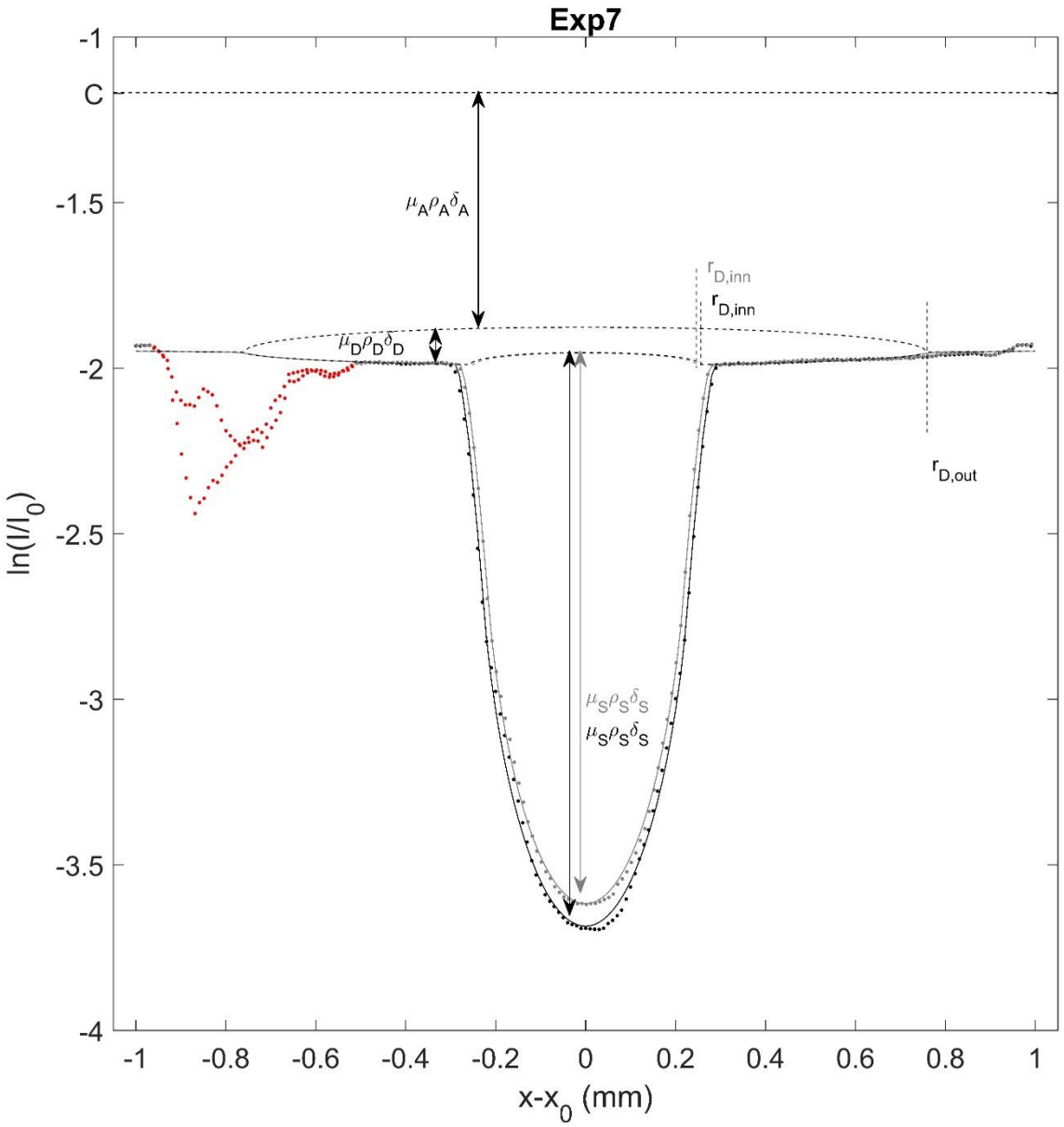

Figure 3. Two profiles of *in situ* (PT) X-ray absorption data of Exp7 (black and grey dots), which are taken at different altitude, and their fits (black and grey solid lines). Measurements that are affected by absorption of MgO+Pt calibrant powder are plotted in red and excluded from the fit. Dashed lines represent the separate components of the absorption, i.e. absorption by gain differences of the diodes (C), the assembly's absorption (A), the diamond's absorption

(D) and the sample's absorption (S). Raw data and the beer-lambert parametrisations are available online (Knibbe, 2020).

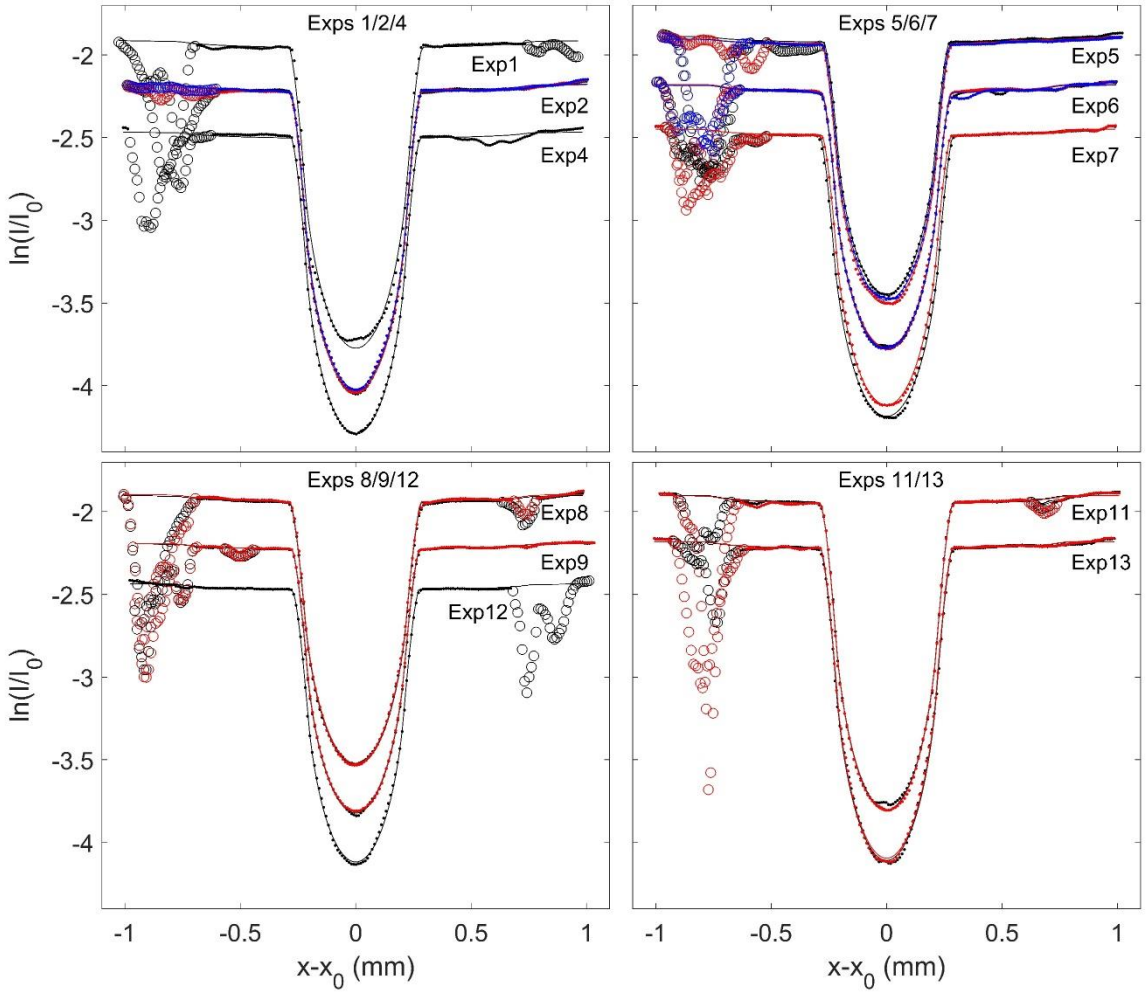

Figure 4. The *in situ* (PT) X-ray absorption profiles (dotted) of the assembly, diamond and sample. The Beer-Lambert parametrisation that is fitted to the absorption profiles (solid lines). Measurements that are considered as outliers, of which most are affected by absorption of MgO+Pt calibrant powder at the outside of the diamond cylinder, are plotted as open circles and are excluded from the fit. The profiles and the fits are artificially shifted along the Y-axis for illustrative purposes. Most experiments yielded more than one PT absorption profile at different vertical positions, which are distinguished by colour (black, red and blue). Raw data and the beer-lambert parametrisation are available online (Knibbe, 2020).

Experiment-set	Experiment	$\rho_{S,0}\mu_{S,0}$ (m^{-1})	$\rho_{S,PT}\mu_{S,PT}$ (m^{-1})
Exp1/2/4	Exp1	3895 (6)	3678 (20)
	Exp2	3895 (6)	3724 (4)
	Exp4	3895 (6)	3747 (12)
Exp5/6/7	Exp5	3508 (3)	3263 (3)
	Exp6	3508 (3)	3202 (4)

	Exp7	3508 (3)	3387 (7)
Exp8/9/12	Exp8	3588 (4)	3254 (5)
	Exp9	3588 (4)	3371 (3)
	Exp12	3588 (4)	3517 (7)
Exp11/13	Exp11	4091 (5)	3777 (6)
	Exp13	4091 (5)	3840 (7)

Table 1. Fitting results. Formal fitting errors are noted between brackets.

3. Hydrostatic Weighing

The density of recovered samples $(\rho_{S,0})$ is measured by hydrostatic weighing (e.g., Neuville, 2006) in diiodomethane liquid at the Institute de Physique du Globe Paris (IPGP) in Paris, France. By the principle of Archimedes, the density of the recovered sample is given by

$$\rho_{S,0} = \rho_l \frac{m_a}{m_a - m_l}, \qquad (A6)$$

with ρ_l the density of the liquid, m_a the apparent mass of the sample in air and m_l the apparent mass of the sample immersed in the liquid. The temperature of diiodomethane was measured at 30.6 °C by a mercury thermometer and did not vary between the measurements by more than 0.2 °C. Diiodomethane liquid has a density (ρ_l) of 3.2935 g·cm^{-3} at this temperature (Griffing et al., 1954). A high-precision balance of 10^{-5} g resolution is used to measure m_a and m_l. The precision limit of the balance propagates to a maximum accuracy on $\rho_{S,0}$ of ~ ± 0.2 g·cm^{-3} on our single samples of ~ $50 \cdot 10^{-5}$ g. To increase the precision of the density measurement, we assume that recovered samples from the same starting composition have the same density. We weigh the sets of samples that shared the starting composition as an ensemble. Samples of Exp2, Exp5, Exp7 and Exp9 have unfortunately been lost during the weighing process, and their densities are assumed equal to the average density that is measured on recovered samples that shared the starting composition. The results of the hydrostatic weighing are summarized in table A2.

Sample group	Weighed samples	m_a (10^{-5}g)	m_l (10^{-5}g)	$\rho_{S,0}$ (g·cm^{-3})
Exp11/13	Exp11 and Exp13	122.5(0.5)	67.5(0.5)	7.34(0.10)
Exp1/2/4	Exp1 and Exp4	117.5(0.5)	63.5(0.5)	7.17(0.10)
Exp8/9/12	Exp8 and Exp12	111.5(0.5)	58.0(1.0)	6.86(0.15)
Exp5/6/7	Exp6	55.5(0.5)	27.5(0.5)	6.53(0.18)

Table 2. This table lists the results of the hydrostatic weighing and the samples that are used in the hydrostatic weighing. The uncertainty is listed in brackets.

4. Pressure and temperature conditions

The pressure and temperature conditions of the measurements at experimental (PT) conditions are determined by crossings of the isochores that correspond to the unit cell volumes of the Pt and BN calibrant materials. These unit cell volumes are derived from *in-situ* collected X-ray

absorption spectra of the Pt and BN. The equation of states of Pt from Fei et al. (2007) and of BN from Wakabayashi and Funamori (2015) are used to compute the isochores (table 3). Expected uncertainties on the isochore crossings are ± 0.5 GPa and ± 150 K.

Experiment	Oil P (bar)	Power (W)	a_{Pt} (Å)	a_{BN} (Å)	c_{BN} (Å)	Sample P (GPa)	Sample T (K)
Exp1	300	340	3.958	2.4975	6.358	3.27	1607
Exp2	400	300	3.959	2.496	6.276	4.18	1748
Exp4	500	290	3.955	2.4945	6.1255	5.89	1869
Exp5	300	310	3.9705	2.4968	6.3435	3.92	1984
Exp6	400	320	3.957	2.495	6.225	3.36	1908
Exp7	500	330	3.956	2.4948	6.15	5.59	1999
Exp8	300	330	3.97	2.4975	6.398	3.36	1901
Exp9	400	330	3.97	2.497	6.309	4.23	2012
Exp11	300	300	-	2.498	6.352	3.92	1984
Exp12	500	310	3.9598	2.4945	6.15	5.78	1972
Exp13	400	310	-	2.4975	6.2995	4.23	1906

Table 3. Lattice parameters of BN and Pt are derived from *in situ* X-ray spectra that are made available online (Knibbe, 2020). Pressure and temperature are estimated by isochore crossings using equation of states of Pt from Fei et al. (2007) and of BN from Wakabayashi and Funamori (2015). For Exp6 and Exp7, the listed lattice parameters correspond to calibrant spectra taken at subliquidus conditions, because the spectra at the superliquidus conditions of the absorption measurements did not provide a good Pt signal. Temperature is extrapolated to the absorption measurement conditions by assuming an increase of temperature that is proportional to the applied electrical power. The Pt signals were also absent for Exp11 and Exp13, for which we assume identical sample pressure as Exp5 and Exp9, respectively, based on the similar power, oil pressure and BN lattice parameter. Temperatures of Exp11 and Exp13 are power-corrected relative to the temperatures Exp5 and Exp9.

5. Uncertainties

We tested the sensitivity of our results to modelling assumptions by trial and error and noticed that the formal fitting errors (table 1) are poor indicators of the accuracy of $\rho_S\mu_S$. For example, the estimate of $\rho_S\mu_S$ corresponding to ambient-pressure absorption data of Exp5, Exp6, and Exp7 (figure 2) is 3509 m^{-1} with a formal standard error of 3 m^{-1}. When we fix the width of the beam (L) to the slits-controlled dimension of 0.1 mm instead of fitting L to the data, an estimate for $\rho_S\mu_S$ of 3560 m^{-1} with a formal standard error of 4 m^{-1} is obtained. We have more confidence in the fitted estimate of L, which is consistently estimated at 0.06-0.07 mm for the acquired data in this study. The difference between the fitted value of L and the slits-controlled target value is on the order of the precision on the calibration of the slit-window (normally ±0.02 mm at this beamline), such that a smaller beam width compared to the target value is possible. The corresponding difference in the fitting result indicates that model assumptions, instead of fitting errors, dominate the actual uncertainties on $\rho_S\mu_S$. By testing the influence of this and several other model assumptions, the obtained estimates of $\rho_S\mu_S$ vary by up to ~ 2 %. For this reason,

we adopt a standard error of 2 % on estimates of $\rho_S \mu_S$ instead of the formal fitting errors that are listed in table 1.

We recall that it was necessary to weigh samples that share the identical starting composition together (as a set) under the assumption that their ambient-condition sample densities $(\rho_{S,0})$ are identical. This resulted in that also the estimated values of $\rho_{S,0}\mu_S$ are identical among such a set of samples (section 2.2). To estimate the errors that are related to this assumption, we fitted individual values of $\rho_{S,0}\mu_S$ to the ambient-condition absorption profiles of individual experiments, and obtained estimates of $\rho_{S,0}\mu_S$ for individual experiments which deviate from the values that are reported in table 1 by less than 1 %. It is inconsistent with the adopted assumption to use these experiment-specific estimates of $\rho_{S,0}\mu_S$ for calculating the density of the sample at experimental conditions.

An additional error is related to a difference between composition of individual samples relative to the adopted average composition of samples that shared their starting mixtures. The compositional variation among each set of measured samples is < ± 1 wt% Si (determined by microprobe measurements). According to the derived mixing models (text D), this compositional variation corresponds to a density deviation of below ± 50 kg·m^{-3} (< ± 1 %) compared to the average density of the corresponding set of samples. This deviation is consistent with the variability in $\rho_{S,0}\mu_S$ of below 1 % of individual absorption profiles that are collected at ambient pressure.

References

Fei, Y., Ricolleau, A., Frank, M., Mibe, K., Shen, G., & Prakapenka, V. (2007), Toward an internally consistent pressure scale, *Proceedings of the National Academy of Sciences of the united States of America*, *104*(22), 9182-9186, doi:10.1073/pnas.0609013104.

Griffing, V., Cargyle, M. A., Corvese, L., & Eby, D. (1954), Temperature coefficients of viscosity of some halogen substituted organic compounds, *The Journal of Physical Chemistry*, *58*(11), 1054-1056, doi:10.1021/j150521a032.

Knibbe, J. S. (2020). supplementary data to "Mercury's Interior Structure constrained by Density and P-wave Velocity Measurements of Liquid Fe-Si-C Alloys" [Data set], *Zenodo*, doi:10.5281/ZENODO.4090496.

Knibbe, J. S., Rivoldini, A., Luginbuhl, S., Namur, O., Charlier, B., Mezouar, M., Berndt, J., Kono, Y., Neuville, D., van westrenen, W., and Van Hoolst, T., (2020, in press), Mercury's Interior Structure constrained by Density and P-wave Velocity Measurements of Liquid Fe-Si-C Alloys, *Journal of Geophysical Research: Planets*, doi: 10.1029/2020JE006651.

Neuville, D. R. (2006), Viscosity, structure, and mixing in (Ca, Na) silicate melts, *Chemical Geology*, *229*(1-3), 28-41, doi:10.1061/j.chemgeo.2006.01.008.

van Kan-Parker, M., Sanloup, C., Tronche, E. J., Perrilat, J. -P., Mezouar, M., Rai, N., & van Westrenen, W. (2010), Calibration of a diamond capsule cell assembly for in situ determination of liquid properties in the Paris-Edinburgh press, *High Pressure Research*, *30*(2), 332-341, doi: 10.1080/08957959.2010.484283.

Wakabayashi, D. & Funamori, N. (2015), Solving the problem of inconsistency in the reported equations of state for h-BN, *High Pressure Research*, *35*(2), 123-129, doi: 10.1080/08957959.2015.1028931.